LIMIT CYCLES IN EMBEDDED HIGH-ORDER, LOWPASS SIGMA-DELTA MODULATORS WITH DISTINCT NTF ZEROS

Ngai Wong and Tung-Sang Ng

Department of Electrical and Electronic Engineering,
The University of Hong Kong, Pokfulam Road, Hong Kong.
nwong@eee.hku.hk, tsng@eee.hku.hk
Tel.: ++ 852 + 2857 8406, Fax: ++ 852 + 2559 8738

Abstract: In a related work by the authors, high-order sigma-delta ($\Sigma\Delta$) modulators with distinct noise transfer function (NTF) zeros are decomposed into second-order and first-order subsystems, whose state-trajectories are then investigated by continuous-time embedding. This paper, based on the properties of these subsystems, furthers the study by introducing a scalable numerical method to locate the fixed-points on the generalized Poincaré sections. Closed-form tangent linear manifold matrix for an arbitrary order modulator is derived, enabling the stability determination of the fixed-points and the accompanying limit cycles. Numerical examples show that the estimated DC input bound based on the boundary transition flow assumption cannot be relied on for modulators of order greater than four.

1. INTRODUCTION

In a previous paper by the authors [1], it has been shown that by extending the state-space analysis framework of Steiner and Yang [2], high-order, lowpass, single-bit sigma-delta ($\Sigma\Delta$) modulators with distinct NTF zeros can be transformed and decomposed into individual second-order and first-order subsystems. In the phase plot of this new framework, a second-order subsystem represents an anti-clockwise trajectory circling about two half-plane centers while a first-order subsystem represents an oscillating quantity in the vertical sense. The switching of dynamics is determined by the summation of the vertical coordinate components of all subsystem trajectories [1]. Continuous-time embedding of Wang [3] has been applied and generalized to include different transition flows, and the corresponding Poincaré section expressions have been given.

Under stable DC operation of a $\Sigma\Delta$ modulator, these subsystem trajectories are coupled in a way that they counteract each other. Section 2 of this paper shows that this coupling results in two sets of horizontal lines, denoted as the *positive* and *negative threshold lines*. The sum of these threshold lines corresponds to the hyperplane $\boldsymbol{P}$ separating the dynamics of a $\Sigma\Delta$ modulator into two half-planes, called the positive half-plane ***PHP*** and the negative half-plane ***NHP***, wherein the quantizer output is positive and negative respectively. The state-trajectory within these half-planes, being affine, can be solved linearly. By exploiting the properties of these subsystems, Section 3 constructs a system of nonlinear equations and suggests an efficient numerical method to solve for the fixed-points lying on the generalized Poincaré sections of a particular transition flow. Section 4 derives a scalable tangent linear manifold matrix that enables the judgment of the fixed-point stability and the limit cycles thus formed. Through numerical examples, it is then shown that the estimation of the DC input bound based on the boundary transition flow assumption of Wang [3] is not reliable for modulators of order greater than four. Concluding remarks are drawn in Section 5.

2. SUBSYSTEM COUPLING

Using the results and notations from [1], a decomposed, continuous-time embedded N th-order ($N>2$) $\Sigma\Delta$ modulator is interpreted as separate second-order subsystems, plus an additional first-order subsystem when N is odd. The i th second-order subsystem has circular trajectories orbiting with an "angular speed" ω_i about two half-plane centers: $(-\omega_i^{-1}\alpha_{2i},\ \omega_i^{-1}\alpha_{2i-1})$ for the ***PHP*** and $(\omega_i^{-1}\alpha_{2i},\ -\omega_i^{-1}\alpha_{2i-1})$ for the ***NHP*** (here α_i stands for the i th element in the $N\times 1$ feedback vector in the continuous-time state-space model). Whereas when N is odd, the one first-order subsystem is characterized by a quantity traveling at a "speed" of $\gamma_+ \equiv \beta_N u+\alpha_N$ in the ***PHP*** and $\gamma_- \equiv \beta_N u-\alpha_N$ in the ***NHP*** (here β_i stands for the i th element in the $N\times 1$ input vector in the continuous-time state-space model and u is the DC input).

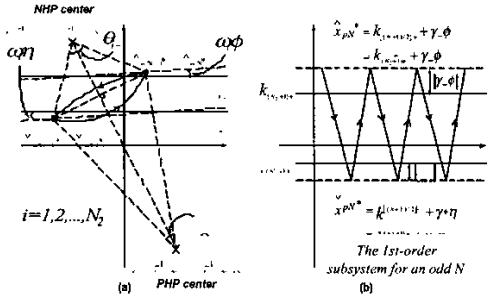

*Fig. 1. Limit cycles in subsystems: **(a)** second-order; **(b)** first-order.*

Fig. 1 shows typical limit cycles in subsystems under stable DC input and practical examples can be found in [1]. The positive and negative threshold lines, denoted

by k_{i+}s and k_{i-}s, satisfy the condition for the trajectories to be on the hyperplane $\boldsymbol{P}$, namely,

$$\sum_{i=1}^{\lfloor (N+1)/2 \rfloor} k_{i+} = \sum_{i=1}^{\lfloor (N+1)/2 \rfloor} k_{i-} = -Ku \tag{1}$$

where the floor function $\lfloor (N+1)/2 \rfloor$ gives the total number of decomposed subsystems (inclusive of second-order and first-order ones). Also, the number of second-order subsystems is $N_2 = \lfloor N/2 \rfloor$. The positive threshold lines represent the thresholds across which a trajectory enters the ***PHP*** and the negative threshold lines denote the thresholds for entering the ***NHP***. The discrete nature of practical $\Sigma\Delta$ modulators will carry the trajectory forward after hitting $\boldsymbol{P}$, penetrating into a region in the ***PHP*** (***NHP***) called the positive transition wedge $\hat{T}$ (negative transition wedge $\check{T}$) just before changing dynamics. As a generalization to cover all possible transition flows [3], a trajectory will go on for ϕ and η more time-step ($\phi, \eta \in [0,1]$, i.e., rotate for $\omega_i\phi$ and $\omega_i\eta$ more radians in a second-order subsystem or proceed for $\gamma_-\phi$ and $\gamma_+\eta$ more distance for a first-order subsystem) onto the (generalized) Poincaré sections $\hat{P}_\phi$ and $\check{P}_\eta$, landing on the two fixed-points [3] $\hat{\mathbf{x}}_\mathbf{p}^* = [\hat{x}_{p1}^* \cdots \hat{x}_{pN}^*]$ and $\check{\mathbf{x}}_\mathbf{p}^* = [\check{x}_{p1}^* \cdots \check{x}_{pN}^*]$ respectively. Strictly speaking, the parameters ϕ and η should be included in the notations of $\hat{\mathbf{x}}_\mathbf{p}^*$ and $\check{\mathbf{x}}_\mathbf{p}^*$ but they are omitted for simplicity and should be obvious from the context. Referring to Fig. 1, it can be verified that,

$$\hat{x}_{p2i}^* = (\hat{x}_{p2i-1}^* - \omega_i^{-1}\alpha_{2i})\tan\omega_i\phi + \frac{k_{i+} + \omega_i^{-1}\alpha_{2i-1}}{\cos\omega_i\phi} - \omega_i^{-1}\alpha_{2i-1} \tag{2}$$

and

$$\check{x}_{p2i}^* = (\check{x}_{p2i-1}^* + \omega_i^{-1}\alpha_{2i})\tan\omega_i\eta + \frac{k_{i-} - \omega_i^{-1}\alpha_{2i-1}}{\cos\omega_i\eta} + \omega_i^{-1}\alpha_{2i-1} \tag{3}$$

for $i = 1,2,\ldots,N_2$. As for the first-order subsystem,

$$\hat{x}_{pN}^* = k_{(N_2+1)+} + \gamma_-\phi \quad \text{and} \quad \check{x}_{pN}^* = k_{(N_2+1)-} + \gamma_+\eta\,. \tag{4}$$

For completeness, the expressions for the fixed-points on the two Poincaré sections are quoted here [1]:

$$\hat{P}_\phi : \left(\sum_{i=1}^{N_2} -(\hat{x}_{p2i-1}^* - \omega_i^{-1}\alpha_{2i})\sin\omega_i\phi + (\hat{x}_{p2i}^* + \omega_i^{-1}\alpha_{2i-1})\cos\omega_i\phi - \omega_i^{-1}\alpha_{2i-1} \right) \Big| + \hat{x}_{pN}^* - \gamma_-\phi = -Ku \tag{5}$$

and

$$\check{P}_\eta : \left(\sum_{i=1}^{N_2} -(\check{x}_{p2i-1}^* + \omega_i^{-1}\alpha_{2i})\sin\omega_i\eta + (\check{x}_{p2i}^* - \omega_i^{-1}\alpha_{2i-1})\cos\omega_i\eta + \omega_i^{-1}\alpha_{2i-1} \right) \Big| + \check{x}_{pN}^* - \gamma_+\eta = -Ku \tag{6}$$

where the last summations after the vertical delimiting lines in (5) & (6) are present for odd-order modulators (odd Ns) only, and K is the forward-path resonator DC gain [1]. This convention of combined representation will be followed throughout this paper.

3. LOCATING FIXED-POINTS

Supposed the threshold lines are given, the fixed-points for each second-order subsystem, with the help of (2) & (3) and the fact that the fixed-points and the two half-plane centers must form into a symmetrical kite shape as in Fig. 1, can be solved by two simultaneous equations:

$$\begin{cases} (\tan\omega_i\phi + \alpha_{2i-1}/\alpha_{2i})\hat{x}_{p2i-1}^* + (\tan\omega_i\eta + \alpha_{2i-1}/\alpha_{2i})\check{x}_{p2i-1}^* = \\ \quad \omega_i^{-1}\alpha_{2i}(\tan\omega_i\phi - \tan\omega_i\eta) - \dfrac{k_{i+} + \omega_i^{-1}\alpha_{2i-1}}{\cos\omega_i\phi} - \dfrac{k_{i-} - \omega_i^{-1}\alpha_{2i-1}}{\cos\omega_i\eta} \\ (\tan\omega_i\phi - \alpha_{2i}/\alpha_{2i-1})\hat{x}_{p2i-1}^* - (\tan\omega_i\eta - \alpha_{2i}/\alpha_{2i-1})\check{x}_{p2i-1}^* = \\ \quad \omega_i^{-1}\alpha_{2i}(\tan\omega_i\phi + \tan\omega_i\eta) - \dfrac{k_{i+} + \omega_i^{-1}\alpha_{2i-1}}{\cos\omega_i\phi} + \dfrac{k_{i-} - \omega_i^{-1}\alpha_{2i-1}}{\cos\omega_i\eta} + 2\omega_i^{-1}\alpha_{2i-1} \end{cases} \tag{7}$$

where $i = 1,2,\ldots,N_2$. For each second-order subsystem, the positive and negative fly-times [the time that the trajectory spends in ***PHP*** and ***NHP*** respectively, *p_time* and *n_time* in (8)] can then be obtained by dividing the angles sustained about each half-plane center (θ_{i+} and θ_{i-} in Fig. 1) by ω_i, giving

$$\begin{cases} p\_time_i(\hat{x}_{p2i-1}^*, \hat{x}_{p2i}^*, \check{x}_{p2i-1}^*, \check{x}_{p2i}^*) \\ \quad = \dfrac{1}{\omega_i}\arg\left(\dfrac{(\check{x}_{p2i-1}^* + \omega_i^{-1}\alpha_{2i}) + j(\check{x}_{p2i}^* - \omega_i^{-1}\alpha_{2i-1})}{(\hat{x}_{p2i-1}^* + \omega_i^{-1}\alpha_{2i}) + j(\hat{x}_{p2i}^* - \omega_i^{-1}\alpha_{2i-1})} \right) \\ n\_time_i(\hat{x}_{p2i-1}^*, \hat{x}_{p2i}^*, \check{x}_{p2i-1}^*, \check{x}_{p2i}^*) \\ \quad = \dfrac{1}{\omega_i}\arg\left(\dfrac{(\hat{x}_{p2i-1}^* - \omega_i^{-1}\alpha_{2i}) + j(\hat{x}_{p2i}^* + \omega_i^{-1}\alpha_{2i-1})}{(\check{x}_{p2i-1}^* - \omega_i^{-1}\alpha_{2i}) + j(\check{x}_{p2i}^* + \omega_i^{-1}\alpha_{2i-1})} \right) \end{cases} \tag{8}$$

where $i = 1,2,\ldots,N_2$ and $\arg(\cdot)$ is the angle function of a complex quantity. For the first-order subsystem in an odd-order modulator, its fixed-points as a function of the threshold lines are simply (4). And the fly-times

$$\begin{cases} p\_time_{N_2+1}(\hat{x}_{pN}^*, \check{x}_{pN}^*) = (\check{x}_{pN}^* - \hat{x}_{pN}^*)/\gamma_+ \\ n\_time_{N_2+1}(\hat{x}_{pN}^*, \check{x}_{pN}^*) = (\hat{x}_{pN}^* - \check{x}_{pN}^*)/\gamma_- \end{cases} \tag{9}$$

In (7)-(9), all but the threshold lines are fixed for a given modulator and transition flow assumption. The threshold lines therefore completely characterize the fixed-points and fly-times of each subsystem. Functions can be constructed in terms of them to locate the fixed-points when all the subsystems are coupled. Due to the nonlinearity in those functions thus formed, they are best solved by numerical methods. The approach is based on writing generic modules for each subsystem. These modules work like nonlinear functions that generate the fixed-points and fly-times given the threshold lines and other parameters like the centers and angular speed etc. The module for a second-order subsystem is as follows:

module: second_order_system$(k_{i+}, k_{i-}, \omega_i, \alpha_{2i-1}\alpha_{2i}, \phi, \eta)$

$$\begin{bmatrix} \textit{Solve for } \hat{x}_{p2i-1}^*, \hat{x}_{p2}^*, \check{x}_{p2i-1}^*, \check{x}_{p2i}^* \textit{ based on (33);} \\ \textit{Solve for } p\_time_i, n\_time_i \textit{ based on (34).} \end{bmatrix} \tag{10}$$

return $[\hat{x}_{p2i-1}^*, \hat{x}_{p2i}^*, \check{x}_{p2i-1}^*, \check{x}_{p2i}^*, p\_time_i, n\_time_i]$

for $i = 1,2,\ldots,N_2$. Whereas for the first-order subsystem:

module: first_order_system$(k_{[N_2+1)/2+}, k_{[N_2+1)/2-}, \gamma_+, \gamma_-, \phi, \eta)$ (11)

$\begin{cases} \text{Solve for } \hat{x}_{p1}^{*}, \check{x}_{p1}^{*} \text{ based on (35);} \\ \text{Solve for } p\_time_{N_2+1}, n\_time_{N_2+1} \text{ based on (36).} \end{cases}$

return $[\hat{x}_{p1}^{*}, \check{x}_{p1}^{*}, p\_time_{N_2+1}, n\_time_{N_2+1}]$

Finding the limit cycles when these individual subsystems are coupled is equivalent to solving for the following set of nonlinear equations in terms of the threshold line values k_{i+}, k_{i-} (i = 1,2,...,$\lfloor (N+1)/2 \rfloor$) such that all subsystems give the same positive and negative fly-times, namely,

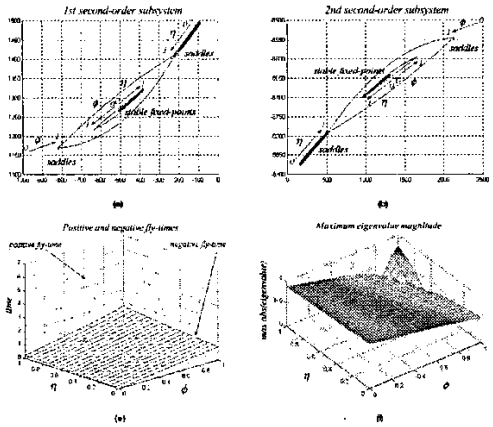

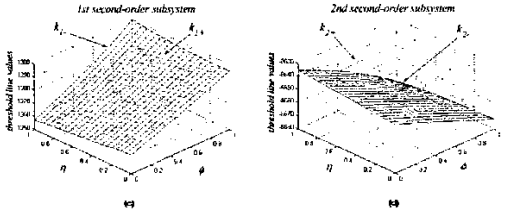

Fig. 2. *An example continuous-time embedded 4th-order modulator (input 0.595, oversampling ratio 64, optimized NTF zeros):* ***(a)*** *&* ***(b)*** *fixed-points found numerically for different transition flows;* ***(c)*** *&* ***(d)*** *threshold line values corresponding to stable fixed-points;* ***(e)*** *positive and negative fly-times for stable limit cycles;* ***(f)*** *maximum eigenvalue magnitude for the tangent linear manifolds of stable fixed-points.*

$$\mathbf{G}=\left[g_1 \;\; g_2 \;\; \cdots \;\; g_{2\lfloor (N+1)/2 \rfloor-1} \;\; g_{2\lfloor (N+1)/2 \rfloor}\right]^T \quad \text{where}$$
$$\begin{cases} g_{2i-1} = p\_time_i(k_{i+}, k_{i-}) - p\_time_{i+1}(k_{i+1)+}, k_{(i+1)-}) \\ g_{2i} \;\; = n\_time_i(k_{i+}, k_{i-}) - n\_time_{i+1}(k_{i+1)+}, k_{(i+1)-}) \end{cases} \quad (12)$$

i =1,2,...,$\lfloor (N+1)/2 \rfloor$-1 such that there are $2\lfloor (N+1)/2 \rfloor$ unknowns (the k_{i+}'s and k_{i-}'s). The objective is to find a vector $\mathbf{k}=[k_{1+} \;\; k_{1-} \cdots k_{\lfloor (N+1)/2 \rfloor+} \;\; k_{\lfloor (N+1)/2 \rfloor-}]^T$ holding all threshold line values such that $\mathbf{G}=\mathbf{0}$, i.e., the condition for a global limit cycle. But from (1),

$$k_{\lfloor (N+1)/2 \rfloor+} = -Ku - \sum_{i=1}^{\lfloor (N+1)/2 \rfloor-1} k_{i-} \quad \text{and} \quad k_{\lfloor (N+1)/2 \rfloor-} = -Ku - \sum_{i=1}^{\lfloor (N+1)/2 \rfloor+1} k_{i-}, \quad (13)$$

thus the last two elements in $\mathbf{k}$ are functions of the other elements as in (13). So effectively there are $2(\lfloor (N+1)/2 \rfloor - 1)$ equations with the same number of unknowns, which can then be solved numerically. The Broyden's method [5] is chosen for such purpose due to its reduced complexity and superlinear convergence. In (12) the fly-times of the first subsystem is used as the reference to equate all other subsystems' fly-times. This is observed to give faster convergence in our choice of numerical method than by equating the fly-times of every two adjacent subsystems. The initial condition to kick off the Broyden's algorithm, which is an approximate solution, can be easily estimated from simulation. Fig. 2 shows the fixed-points, threshold lines, and fly-times thus obtained for an example 4th-order modulator against all transition flows. By varying the initial conditions in the Broyden's algorithm, two sets of fixed-points can be found. Using results from the next section, the "inner" set stands for those stable fixed-points while the "outer" set represents saddles with unstable limit cycles. The fixed-points and threshold lines for the first-order subsystem in an odd-order modulator is structured similarly and omitted to restrict the length of this paper. In loose terms, there exists a region (constituting the domain of attraction) between the inner stable limit cycles and the outer unstable ones where trajectories (if started with an appropriate initial condition) will be "repelled" back to the stable limit cycles. Trajectories going beyond the saddles will swirl away and result in instability (unbounded) or even chaotic behavior (bounded). It can also be seen that the boundary transition flow ($\phi=\eta=1$) suggested by Wang [3] has the "least-forgiving" or the smallest attracting region between the stable fixed-points and the saddles.

4. STABILITY OF LIMIT CYCLES

A standard technique of evaluating the stability of the Poincaré section fixed-points is to investigate the tangent linear manifolds (lying on $\hat{P}_\phi$ and $\check{P}_\eta$) about them. Such approach requires the availability of closed-form, time-independent algebraic functions for the trajectory evolution within each half-plane. This is possible by utilizing the subsystem properties as described. Recognizing the Poincaré map, denoted by $\Re : \hat{\mathbf{x}}_\mathbf{p} \rightarrow \hat{\mathbf{x}}_\mathbf{p}' = (\Re : \hat{\mathbf{x}}_\mathbf{p} \rightarrow \check{\mathbf{x}}_\mathbf{p}) \circ (\Re : \check{\mathbf{x}}_\mathbf{p} \rightarrow \hat{\mathbf{x}}_\mathbf{p}')$ (where $\hat{\mathbf{x}}_\mathbf{p} = [\hat{x}_{p1} \cdots \hat{x}_{pN}]$ and $\check{\mathbf{x}}_\mathbf{p} = [\check{x}_{p1} \cdots \check{x}_{pN}]$ etc. are the state-variables within each half-plane) as a two-step return map, starting with the ***PHP***, the first set of functions is related to the circular constraint for the trajectories of second-order subsystems,

$$\hat{f}_i(\hat{\mathbf{x}}_p,\check{\mathbf{x}}_p)=(\hat{x}_{p2i-1}+\omega_i^{-1}\alpha_{2i})^2+(\hat{x}_{p2i}-\omega_i^{-1}\alpha_{2i-1})^2 - (\check{x}_{p2i-1}+\omega_i^{-1}\alpha_{2i})^2-(\check{x}_{p2i}-\omega_i^{-1}\alpha_{2i-1})^2 \quad (14)$$

for $i = 1,2,\ldots,N_2$. The second set of functions describes the fly-time difference of every two adjacent subsystems,

$$\hat{f}_{N_2+i}(\hat{\mathbf{x}}_p,\check{\mathbf{x}}_p)=p\_time_i(\hat{\mathbf{x}}_p,\check{\mathbf{x}}_p)-p\_time_{i-1}(\hat{\mathbf{x}}_p,\check{\mathbf{x}}_p) \quad (15)$$

for $i = 1,2,\ldots,N_2-1$ (or N_2 for odd-ordered modulators). Finally there are two equations quantifying the "exactness" of $\hat{\mathbf{x}}_p$ and $\check{\mathbf{x}}_p$ on $\hat{P}_\phi$ and $\check{P}_\eta$,

$$\hat{f}_N(\hat{\mathbf{x}}_p)=Ku+\left(\sum_{i=1}^{N_2}-(\hat{x}_{p2i-1}-\omega_i^{-1}\alpha_{2i})\sin\omega_i\phi+ +(\hat{x}_{p2i}+\omega_i^{-1}\alpha_{2i-1})\cos\omega_i\phi-\omega_i^{-1}\alpha_{2i-1}\right)\Big|+\hat{x}_{pN}-\gamma\_\phi \quad (16)$$

and

$$\check{f}_N(\check{\mathbf{x}}_p)=Ku+\left(\sum_{i=1}^{N_2}-(\check{x}_{p2i-1}+\omega_i^{-1}\alpha_{2i})\sin\omega_i\eta+ +(\check{x}_{p2i}-\omega_i^{-1}\alpha_{2i-1})\cos\omega_i\eta+\omega_i^{-1}\alpha_{2i-1}\right)\Big|+\check{x}_{pN}-\gamma\_\eta. \quad (17)$$

Clearly (14)-(17) will all become zeros when $\hat{\mathbf{x}}_p$ and $\check{\mathbf{x}}_p$ fall exactly onto the Poincaré sections, i.e.,

$$\hat{f}_i(\hat{\mathbf{x}}_p,\check{\mathbf{x}}_p)\,|_{(\hat{\mathbf{x}}_p^*,\check{\mathbf{x}}_p^*)}=0 \quad \text{for} \quad i=1,2,\ldots,N. \quad (18)$$

Poincaré section analysis reduces the system dimension by one. By setting (16) & (17) to zeros it is possible to derive the differentials of $d\hat{x}_{pN}$ and $d\check{x}_{pN}$ in terms of $d\hat{\mathbf{x}}_{p-1}=[d\hat{x}_{p1}\cdots d\hat{x}_{pN-1}]^T$ and $d\check{\mathbf{x}}_{p-1}=[d\check{x}_{p1}\cdots d\check{x}_{pN-1}]^T$ respectively, namely for an even N,

$$\begin{cases} d\hat{x}_{pN}= \\ \quad \frac{1}{\cos\omega_{N_2}\phi}[\sin\omega_1\phi \;\; -\cos\omega_1\phi\cdots\sin\omega_{N_2-1}\phi \;\; -\cos\omega_{N_2}\phi \;\; \sin\omega_1\phi]d\hat{\mathbf{x}}_{p-1} \\ d\check{x}_{pN}= \\ \quad \frac{1}{\cos\omega_{N_2}\eta}[\sin\omega_1\eta \;\; -\cos\omega_1\eta\cdots\sin\omega_{N_2-1}\eta \;\; -\cos\omega_{N_2-1}\eta \;\; \sin\omega_1\eta]d\check{\mathbf{x}}_{p-1} \end{cases} \quad (19)$$

whereas for an odd N,

$$\begin{cases} d\hat{x}_{pN}=[\sin\omega_1\phi \;\; -\cos\omega_1\phi\cdots\sin\omega_{N_2}\phi \;\; -\cos\omega_{N_2}\phi]d\hat{\mathbf{x}}_{p-1} \\ d\check{x}_{pN}=[\sin\omega_1\eta \;\; -\cos\omega_1\eta\cdots\sin\omega_{N_2}\eta \;\; -\cos\omega_{N_2}\eta]d\check{\mathbf{x}}_{p-1}. \end{cases} \quad (20)$$

Then by partial differentiating the equations in (18) with respect to $\hat{\mathbf{x}}_p$ and $\check{\mathbf{x}}_p$, and substituting $d\hat{x}_{pN}$ and $d\check{x}_{pN}$ by the results in (19) or (20), we arrive at

$$\mathbf{M}_1 d\hat{\mathbf{x}}_{p-1}=\mathbf{M}_2 d\check{\mathbf{x}}_{p-1} \quad (21)$$

where the (i,j)-th element of the $(N-1)\times(N-1)$ matrix $\mathbf{M}_1$ is $\partial\hat{f}_i/\partial\hat{x}_{pj}$ and similarly that of $\mathbf{M}_2$ is $-\partial\hat{f}_i/\partial\check{x}_{pj}$. Likewise, another sets of equations in the ***NHP***, which are counterparts of (18), can be obtained by swapping the symbols $\wedge$ and $\vee$, flipping the half-plane centers in (14), and changing into *n_time* functions in (42). Defining $d\hat{\mathbf{x}}_{p-1}'=[d\hat{x}_{p1}'\cdots d\hat{x}_{pN-1}']^T$ for $(\Re:\ \check{\mathbf{x}}_p\to\hat{\mathbf{x}}_p')$, we have

$$\mathbf{M}_3 d\check{\mathbf{x}}_{p-1}=\mathbf{M}_4 d\hat{\mathbf{x}}_{p-1}' \quad (22)$$

where the (i,j)-th element of the $(N-1)\times(N-1)$ matrix $\mathbf{M}_3$ is $\partial\check{f}_i/\partial\check{x}_{pj}$ and similarly that of $\mathbf{M}_4$ is $-\partial\check{f}_i/\partial\hat{x}_{pj}$. Now combining (21) and (22) and evaluating the matrices at the fixed-points,

$$d\hat{\mathbf{x}}_{p-1}'=\mathbf{M}_4^{-1}\mathbf{M}_3\mathbf{M}_2^{-1}\mathbf{M}_1\big|_{(\hat{x}_p^*,\check{x}_p^*)}\,d\hat{\mathbf{x}}_{p-1} \quad (23)$$

For compactness, we denote $\mathbf{R}=\mathbf{M}_4^{-1}\mathbf{M}_3\mathbf{M}_2^{-1}\mathbf{M}_1|_{(\hat{x}_p^*,\check{x}_p^*)}$. To have stable fixed-points, it is required that all the eigenvalues of $\mathbf{R}$ have magnitude less than unity [3] [c.f. Fig. 2(f)]. Five modulators with different orders are designed and their maximum tangent linear manifold eigenvalue magnitudes, under the boundary transition flow assumption, against different inputs are tabulated in Table 1. Also shown are the DC bounds estimated from 10^5 simulation steps for each modulator. It is evident from the table that relying on the stability of the furthest stretched boundary transition flow can be deceiving since the DC input bound thus estimated (where the maximum eigenvalue magnitude just reaches unity) shows an increasing trend with modulator order greater than four, contradicting the decreasing trend borne out by simulation and experience. Moreover, eigenvalues reaching the magnitude of unity cannot even be found in the third-order modulator. To locate the appropriate DC input bound, it is suggested that all transition flows be considered. The arguments and necessary conditions are summarized in a recent work by the authors [6].

Input u \ Order	3	4	5	6	7
$\lvert eig\rvert_{max}$					
0	0.262	0.518	0.699	0.809	0.871
0.1	0.256	0.512	0.694	0.805	0.869
0.2	0.237	0.495	0.680	0.795	0.860
0.3	0.202	0.461	0.653	0.773	0.843
0.4	0.139	0.399	0.602	0.732	0.811
0.5	0.248	0.243	0.484	0.646	0.752
0.6	0.493	0.799	0.796	0.699	0.693
0.7	0.708	1.442	1.979	2.201	2.263
0.8	0.253				
u @ $\lvert eig\rvert_{max}=1$	N/A	0.631	0.620	0.625	0.629
Simulated bound	0.600	0.633	0.572	0.542	0.523

Table 1. *Numerical results for 5 modulators (optimized NTF zeros, oversampling ratio 64, maximum out-of-band NTF gain 1.5, boundary transition flow assumed).*

5. CONCLUSION

This paper has extended a previous study on the decomposition and state-trajectory behavior of high-order, lowpass ΣΔ modulators with distinct NTF zeros. By exploiting the properties of the decomposed subsystems, this paper has presented the formulation of a set of scalable nonlinear equations governing the trajectories and Poincaré map under different transition flow conditions. This has enabled the solution of fixed-points and the accompanying limit cycles by efficient numerical methods. Closed-form tangent linear manifold essential for stability analysis has also been derived. It has been shown that the DC input bound estimated by assuming boundary transition flow cannot be relied on for modulators of order great than four and further modification is required to derive the accurate bound.

6. REFERENCES

[1] N. Wong and T. S. Ng, "State-trajectory behavior in high-order, lowpass sigma-delta modulators with distinct NTF zeros," submitted to *DSP2002*.

[2] P. Steiner and W. Yang, "A framework for analysis of high-order sigma-delta modulators," *IEEE Trans. Circuits Syst. II*, vol. 44, pp. 1-10, Jan 1997.

[3] H. Wang, "On the stability of third-order sigma-delta modulation," in *Proc. IEEE Int. Symp. Circuits Syst.*, 1993, vol. 2, pp. 1377-1380.

[4] R. Schreier, "An empirical study of high-order single-bit delta-sigma modulators," *IEEE Trans. Circuits Syst. II*, vol. 40, pp. 461-466, Aug 1993.

[5] R. L. Burden and J. D. Faires, *Numerical Analysis*, 7th Ed., Brooks/Cole, 2001.

[6] N. Wong and T. S. Ng, "DC stability analysis of high-order, lowpass sigma-delta modulators with distinct NTF zeros," to be submitted to *IEEE Trans. Circuits Syst. II*.